Variable optical buffer using slow light in semiconductor nanostructures

Pei-Cheng Ku, Connie J. Chang-Hasnain, Jungho Kim, and Shun-Lien Chuang

***Abstract*—We proposed a compact variable all-optical buffer using slow-light in semiconductor nanostructures. We discuss the general design principle via dispersion engineering. The buffering effect is achieved by slowing down the optical signal using an external control light source to vary the dispersion characteristic of the medium via electromagnetically induced transparency effect. We demonstrate that the semiconductor quantum dot structures can be used as a slow-light medium. In such structure, the total buffering time is variable and controlled by an external pump laser. We present a theoretical investigation of the criteria for achieving slow light in semiconductor quantum dots. New pump scheme is proposed to overcome the sample nonuniformity. Finally, optical signal propagation through the semiconductor optical buffer is presented to demonstrate the feasibility for practical applications.**

***Index Terms*—Optical buffer, nanotechnology, quantum optics, integrated optics, quantum dots, packet-switched network**

I. Introduction

A controllable variable optical buffer is one of the most critically sought after components in a next-generation photonic system especially in optical communications and signal processing. An all-optical buffer is the enabling technology for many applications such as all-optical packet switched networks, all-optical signal processing, ultra-low Vπ Mach-Zehnder modulators[1], and *etc*. In such a buffer, optical data would be kept in optical format throughout the storage time without being converted into electronic format. The buffer must be able to turn on to store and off to release optical data at a very rapid rate by an external command. This seemingly simple function to this date has never been realized, in spite of much previous research.

Recently, we proposed a novel approach of making an all-optical buffer in semiconductors[2,3]. Our basic idea centers on making a medium that can controllably slow down optical transmission such that it is effectively an optical memory. By controlling the group velocity reduction factor, the memory storage time can be adjusted to desired values. Our approach involves engineering the material dispersion curve (i.e. refractive index as a function of frequency) with the use of semiconductor nanostructures such as quantum wells (QWs) or quantum dots (QDs) under mechanisms such as electro-magnetically induced transparency[4,5] (EIT) and population oscillation[6].

There have been major breakthroughs recently in achieving slow- or stopped- light in atomic gases and solid-state material using EIT[7,8,9]. Slow-down factors as high as seven orders of magnitude have been demonstrated. Slow-light induced by population oscillation has also been demonstrated in a ruby crystal[10] and in a semiconductor QW[11]. The underlying principle in these experiments is to coherently induce a sharp and pronounced absorption dip in an optical-thick medium to generate a steep dispersion in the index of refraction over a narrow spectral range. The resulting effect is a greatly reduced group velocity and optical absorption for the signal. The reduction of the group velocity scales inversely with the spectral linewidth of the induced transparency window.

This paper is organized as follows. First, we discuss the definition of an optical buffer, followed by a review of various potential applications and previous approaches. Next, we discuss the general principle, i.e. dispersion engineering for the design of a semiconductor optical buffer via slow-light. We then focus on the semiconductor QD-based optical buffer. We will discuss the criteria of semiconductor QDs for attaining the slow-light effect, particularly on homogeneous and inhomogeneous linewidths, and discuss the feasibility to achieve slow light. Device structures are also proposed.

II. All-optical Buffers

A. Definition of optical buffers

We define an optical buffer as a device with both its input and output data streams in optical format without optical-electrical-optical (OEO) conversion. The buffer would store the optical signal for a variable amount of time τ with limited amount of distortion or impairment. Further, the turn on or off should be variable with an external control. We emphasize that only the data stream needs to be all-optical, the header, on the other hand, can have OEO conversion and processed. This is very much in line with what is being used for all-optical cross connect and all-optical networks.

Schematically, an optical buffer can be represented by Fig. 1. The output data stream $f(L,t)$ is essentially a copy of the input data $f(0,t)$; it is equal to the multiple of a proportionality constant p with a time delay τ which is variably controlled by an external source V. L is the length of the device. It is important that signal distortion and dispersion must be within a certain tolerable range to result in a minimum level of impairment. The requirements for other parameters, such as turn on and off times

Pei-Cheng Ku and Connie J. Chang-Hasnain are with the Department of Electrical Engineering and Computer Science, University of California at Berkeley, Berkeley, CA 94720, U.S.A. E-mail: cch@eecs.berkeley.edu .

Jungho Kim and Shun-Lien Chuang are with the Department of Electrical and Computer Engineering, University of Illinois at Urbana-Champaign, 1406 W Green St, Urbana, IL USA 61801

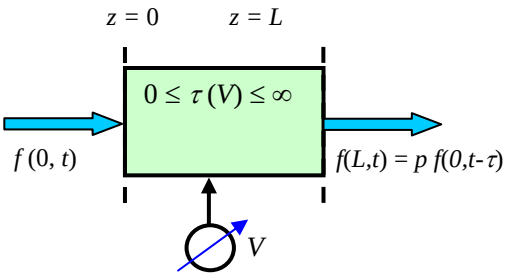

Fig. 1 Definition of an all-optical buffer

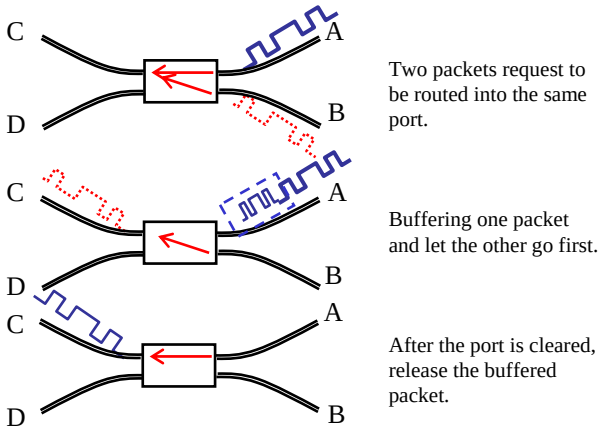

Fig. 2 Optical buffer providing contention resolution in an optical switch.

and optical loss, may vary depending on applications.

B. Potential applications

The most influential application that optical buffers could enable is perhaps all-optical routers in packet-switched networks. A router is used in networks (such as the Internet) to interconnect end-user systems to each other where packets are the basic units of information that are transported. Packet switching is a method of communication whereby information is broken up into blocks of limited length called packets. They are then switched in a network by routers. The blocks can be fixed-length or variable-length but limited. A packet also contains a header, which describes the address of the source and destination for the data. The Internet is a packet-switched network, thus data (in the form of e-mail, a web page, image, news message, etc.) are sent as packets of various lengths and allow many users to share the same data path. In today's network, data are transmitted in optical format and routed and switched in electronic format.

The key building blocks of an electronic router include a switch fabric, processors and buffers. Giving that all-optical switches and signal processing have been demonstrated previously[12], the key missing component for an all-optical router is an all-optical buffer.

Fig. 2 is a schematic showing the function of an optical buffer to resolve contention in an optical switch. With optical buffers, one packet can be stored in the buffer temporarily and let the other packet to go first. Until the traffic is cleared at the output port, the packet stored in the buffer is released. An all-optical router can potentially alleviate the traffic congestion in future very high bandwidth networks.

In addition to the application in optical communication systems, an optical buffer can enable several other possible applications[13] including optical signal processing, RF photonics such as phased-array antennas, nonlinear optics, ultra-low Vπ Mach-Zehnder modulators and time-resolved spectroscopy.

III. Dispersion Engineering

To obtain an optical buffer, in general, one must vary the medium within which the optical signal travels by either increasing the path length or reducing the signal group velocity. The former can be accomplished with the use of a fiber delay line, which will be discussed below. The latter has several possibilities. We first observe that the group velocity v_g is defined as

$$v_g = \frac{\partial \omega}{\partial k} = \frac{c - \omega \dfrac{\partial n(k,\omega)}{\partial k}}{n(k,\omega) + \omega \dfrac{\partial n(k,\omega)}{\partial \omega}} \qquad (1)$$

where n is real part of the refractive index and k is the waveguide propagation constant. We can define a slow down factor S as c/v_g. From (1), we see that the group velocity can be reduced by introducing a large and positive waveguide dispersion $\partial n/\partial k$ or material dispersion $\partial n/\partial \omega$. The waveguide dispersion can be designed using gratings or periodic structure[14,15]. However, to controllability of the group velocity using waveguide dispersion is often severely limited by the narrow range that $\partial n/\partial k$ can be adjusted at a fixed operating wavelength.

On the other hand, reduced group velocity can be achieved via material dispersion by making the term $\partial n/\partial \omega$ positive and large. As we will discuss later, this can be achieved by EIT or population oscillation. The advantage of using material dispersion over waveguide dispersion is the ability to control the group velocity over a wide range simply by the variation of the optical pump intensity.

A. Optical fiber delay lines

Optical fiber delay lines have previously been referred to as "optical buffers"[16]. One most basic design typically consists of a 2 x 2 optical switch connected with a fiber loop (Fig. 3). Other components such as optical isolators, amplifiers and dispersion compensation devices have also been included to reduce impairments due to reflection, loss and dispersion.

The optical switch is first set to direct the data train into the fiber loop and subsequently is closed to allow the data to recirculate in the loop. The storage capacity, i.e. amount of data stored, is limited by the time required to travel one loop τ_{loop}

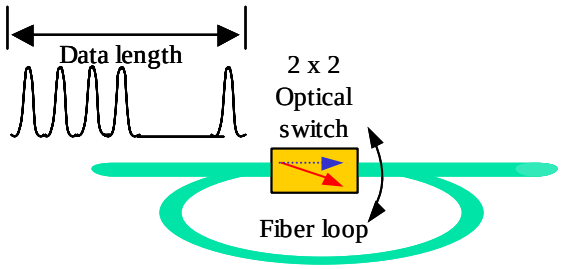

Fig. 3 Fiber delay line used as an optical buffer with fixed storage time[16].

subtracted by that required to set the switch. This is because when the optical data stream is longer than τ_{loop}, the data of the leading part of the packets will overlap with that in the back to cause interference. The storage time, i.e. how long the data is kept in the loop, is an integer multiple of τ_{loop}. The turn off (release) time is also determined by τ_{loop}. This is because once a packet enters the delay line, it can only emerge at a fixed duration of time later. It is impossible to remove the packet from the delay line before that fixed time interval.

The fundamental difficulty facing this design is that the storage time is fixed or quantized by the time required to travel one loop. With the data arrival being random and unsynchronized in real networks, optical routers based on fixed delay times cannot guarantee contention-free connections throughout the network. The fixed time also makes the design of architecture very challenging. These are probably the main reasons why such buffers have not been deployed.

B. Slow-light using waveguide dispersion

Studies on the light propagation in highly dispersive structures with a very slow group velocity have drawn much attention. Grating structures have been used extensively in DFB lasers and grating waveguide couplers. Recent progress on the fabrication of grating structures in fiber has opened new research areas using fiber Bragg gratings[14]. Recently, another method for achieving slowed light based on a Moiré fiber Bragg grating has been suggested[15]. The theoretical analysis shows that the group velocity of light in the transmission band can be slowed down substantially although with a very small signal bandwidth.

C. Slow-light using material dispersion – EIT

Electromagnetically induced transparency (EIT) refers to an artificially created spectral region of transparency in the middle of an absorption line due to the destructive quantum interference arising from two transitions in a three level system[4,5]. There are three basic energy level schemes for implementing a three-level EIT system interacting with two near-resonance electromagnetic fields (Fig. 4)[5]. In all three cases, we label the transitions the same way: |1> to |2>, and |2> to |3> are strong, dipole allowed transitions, while |1> to |3> is a dipole-forbidden transition. The signal field connecting |1> to |2> is the light field

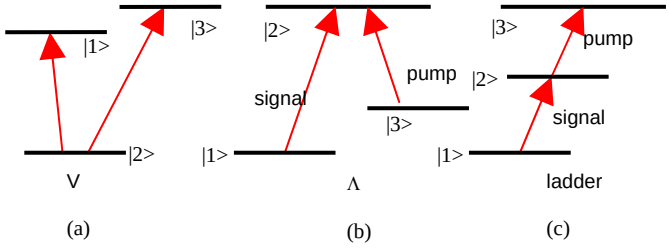

Fig. 4 Three basic schemes for three-level atoms interacting with two near-resonance electromagnetic fields: (a) ladder/cascade (b) Λ, (c) V schemes. In all cases, |1> is dipole coupled to |2> , and |2> to |3> , but |3> is not dipole coupled with |1> (metastable).

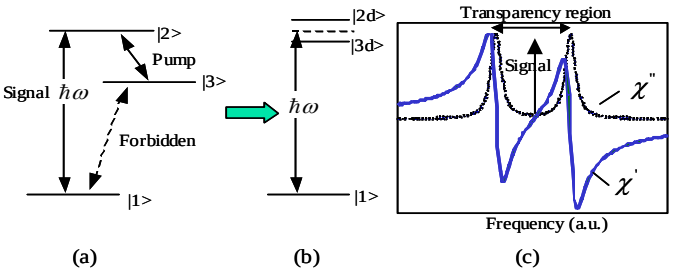

Fig. 5 (a) Λ scheme system with the pump (or coupling or control) laser in the in resonance with states |2> and |3>, results in (b) a set of dressed states |2d> and |3d>. (c) The real (χ') and imaginary (χ") part of susceptibility for the dressed states.

that one desires to slow down in a controllable fashion. The pump field is the control field connecting |2> to |3>, whose intensity controls the amount of slowing down. In the literature, the pump laser is sometimes called the control laser.

As a result of the coherent coupling between the atomic system and the laser beams, atomic levels |1> and |2> are no longer eigen-states of the system. Instead, they are dressed by the pump laser and become two new states |2d> and |3d> (Fig. 5). This (destructive) quantum interference between two absorption paths produces a transparency spectral window in the middle of the strong |1> to |2> absorption line. The width of this transparency window is strongly dependent on the intensity of the pump light field.

By the Kramers-Kronig relations, the induced transparency, which is related to the imaginary part χ" of the optical susceptibility χ, must be accompanied by a dispersive-shaped variation in the real part χ' of the susceptibility (Fig. 5c). Such a variation leads to a very large positive derivative (or gradient) of the index of refraction with respect to frequency inside the center of the EIT transparency region. This slope results in a very large group index of refraction, and thus a reduced group velocity[6-8].

The first demonstrations of ultra-slow and stopped light pulses via EIT were accomplished using atomic vapors, both

ultra-cold and at 80°C, with impressive results[6,7]. Slow-down factors as high as seven orders of magnitude have been demonstrated. Recently, slow and stopped light experiments was

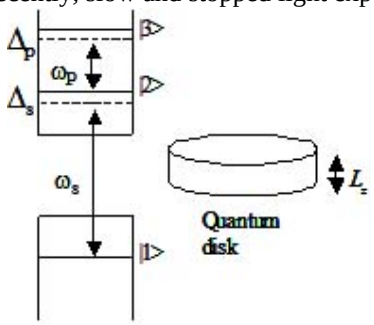

Fig. 6 A quantum disk model used in our calculation.

also achieved in a solid state material at 5K, a praseodymium doped Y_2SiO_5 crystal[8]. In recent years, EIT-like signature was also observed in GaAs/AlGaAs QWs at a temperature as high as 30 K[17-20]. There have been no slow-light experiments reported in semiconductor structures via EIT.

IV. SEMICONDUCTOR QUANTUM DOT OPTICAL BUFFER

Semiconductor quantum dots (QDs) have discrete electronic energy states due to 3D confinement. The discrete energy states make QDs an excellent candidate for slowing down light. There have been many different approaches to make III-V quantum dots. Recently, there have been extensive research efforts on self-assembled growth of QDs on a single crystalline substrate. High quality quantum dots have been achieved in molecular beam epitaxy[21,22], metal-organic chemical vapor deposition[23-25], and atomic layer epitaxy[26].

In this section, we will analyze the slow-light performance in a semiconductor QDs structures. We will first prove the concept by hypothesizing a uniform QD array. We will then propose a new multi-color pump scheme to overcome the non-uniform problem in a realistic QD sample. Signal transmission simulation will be given in the end of this section to demonstrate the feasibility of a QD based optical buffer.

A. Optical Buffer Design

There are many ways to physically construct the slow light "active" region in semiconductor structures. We have chosen a simple 3-level ladder scheme of InAs QD system where |1> is the first heavy hole band, and |2> and |3> are the first two electronic levels in the conduction band, as depicted in Fig. 6. Although this may not be an optimum system that will yield the largest slow-down factor, it is a better known system with the largest amount of characterization data available.

The material parameters listed in Table 1 are calculated from effective-mass approximation for an InAs/GaAs QD system[27]. In this model, the dot is treated as a quantum disk with a radius of 9 nm and a height of 3.5 nm. Band gap shifts due to the biaxial compressive strain are taken into account. The calculated transition wavelengths for the three-level system are 1.36 μm for C1 to HH1 transition, and 12.8 μm for C2-C1 transition, respectively.

As to the device structure, we chose a typical ridge waveguide configuration with multiple QD layers in its

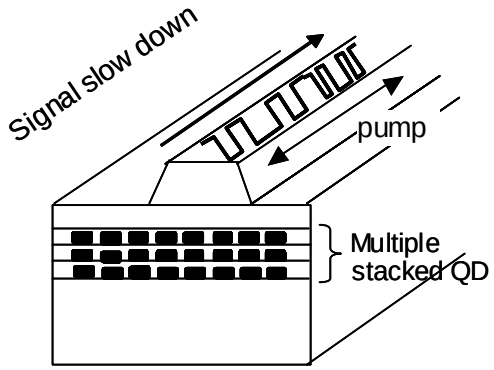

Fig. 7 Schematic of an optical buffer device based on semiconductor quantum dot structures.

Parameters	Values
ω_S	1.36 μm
ω_P	12.8 μm
V	9 nm radius disk and 3.5 nm height
$\lvert\mu_{32}\rvert / e$	24.6 Å
$\lvert\mu_{21}\rvert / e$	21 Å
V / Γ	5×10^3 nm^3

Table 1 Relevant parameters used in the calculation.

waveguide core layer. A schematic of the proposed buffer is given in Fig. 7. The signal and the pump optical beams co-propagate or counter-propagate in the same waveguide. The pump light induces EIT and slows down the signal light velocity.

B. Slow-light in a uniform QD array

To calculate the slow-down factor for a signal propagating in a uniform QD system, we need to know the refractive index change induced by the pump beam. For a three-level system shown in Fig. 6, the time-dependent optical dielectric constant ε experienced by the signal light can be derived from the semi-classical density-matrix ($\langle i|\hat{\rho}|j\rangle$) formulation.

We define the slow-varying density matrices σ_{ij} in terms of the fully time-dependent $\langle i|\hat{\rho}|j\rangle$ as follows.

$$\begin{aligned}\langle 2|\hat{\rho}|1\rangle &= \sigma_{21}e^{-i\omega_s t}\\ \langle 3|\hat{\rho}|2\rangle &= \sigma_{32}e^{-i\omega_p t}\\ \langle 3|\hat{\rho}|1\rangle &= \sigma_{31}e^{-i(\omega_s+\omega_p)t}\end{aligned} \tag{2}$$

The equations of motion for off-diagonal elements σ_{ij} of the density matrix are (rotating-wave approximation has been assumed) as follows.

Temperature (K)	T_2	$\hbar\gamma_H$	Reference
7	630ps	2 μeV	28
25	170ps	7.76 μeV	28
50	37ps	35.6 μeV	28
75	11ps	119.8 μeV	28
100	6ps	219.8 μeV	28
300	290±80fs	4.54meV (3.56 — 6.28 meV)	29

Table 2 Measured dephasing times for various temperatures.

$$\begin{aligned}\dot{\sigma}_{21} &= -(\gamma_{21}+i\Delta_s)\sigma_{21} - i\Omega_s(\rho_{22}-\rho_{11}) + i\Omega_p^*\sigma_{31}\\ \dot{\sigma}_{32} &= -(\gamma_{32}+i\Delta_p)\sigma_{32} - i\Omega_p(\rho_{33}-\rho_{22}) - i\Omega_s^*\sigma_{31}\\ \dot{\sigma}_{31} &= -(\gamma_{31}+i(\Delta_s+\Delta_p))\sigma_{31} + i\Omega_p\sigma_{21} - i\Omega_s\sigma_{32}\end{aligned} \tag{3}$$

The equations of motion for the diagonal elements are as follows.

$$\begin{aligned}\dot{\rho}_{22} &= -\gamma_2\rho_{22} + (\Gamma_{3\to2}\rho_{33} + \Gamma_{1\to2}\rho_{11}) - 2\,\mathrm{Im}(\Omega_s\sigma_{21}^* - \Omega_p\sigma_{32}^*)\\ \dot{\rho}_{33} &= -\gamma_3\rho_{33} + (\Gamma_{2\to3}\rho_{22} + \Gamma_{1\to3}\rho_{11}) - 2\,\mathrm{Im}(\Omega_p\sigma_{32}^*)\\ \dot{\rho}_{11} &= -(\dot{\rho}_{22}+\dot{\rho}_{33})\end{aligned} \tag{4}$$

where the Rabi frequency is $\Omega = \mu E/2\hbar$. $\Gamma_{i\to j}$ accounts for the population transfer rate from state |i> to |j>. The signal and pump detuning are $\Delta_s \equiv \omega_{21} - \omega_S$ and $\Delta_p \equiv \omega_{32} - \omega_P$, respectively. The linewidths are defined as follows

$$\begin{aligned}\gamma_i &= \sum_j \Gamma_{i\to j}\\ \gamma_{ij} &= \frac{1}{2}(\gamma_i+\gamma_j) + \gamma_{ph}\end{aligned} \tag{5}$$

where γ_i and γ_{ph} are lifetime broadening and dephasing broadening linewidths, respectively. Usually, γ_{ph} is the dominant mechanism. Experimentally, γ_{ph} can be measured by the half-width at half maximum (HWHM) homogeneous broadening linewidth $\hbar\gamma_H$. The measured dephasing time in InAs/GaAs QDs and the corresponding linewidth $\hbar\gamma$ are listed in Table 2 below for various temperatures.

At steady state, the solution to (3) gives the macroscopic dielectric constant around the signal frequency solution as follows.

$$\varepsilon_D(\omega\approx\omega_s) = \varepsilon_0\left[\varepsilon_{bac} - i\frac{\Gamma|\mu_{21}|^2}{V\varepsilon_0}\frac{\eta_2}{\tilde{\gamma}_{21}(1+|\Omega_p|^2/\tilde{\gamma}_{21}\tilde{\gamma}_{32})}\right] \tag{6}$$

where Γ is the optical confinement factor and V is the volume of a single QD. $\varepsilon_0 = 8.85\times10^{-12}$ (F/m) and $\varepsilon_0\varepsilon_{bac}$ is the background dielectric constant without coupling to any light. $\eta_2 = \rho_{22} - \rho_{11}$ is the population inversion for level |2>. In (6), the complex detuning $\tilde{\gamma}_{31} = \gamma_{31} + i(\Delta_s+\Delta_p)$ and $\tilde{\gamma}_{21} = \gamma_{21} + i\Delta_s$ are defined. If the condition of EIT is reached, all the photo-created carriers are trapped in the ground state and the term η_2 has only contributions from thermally populated carriers. The group velocity reduction factor can be derived from the first derivative of the dielectric constant with respect to the frequency as follows.

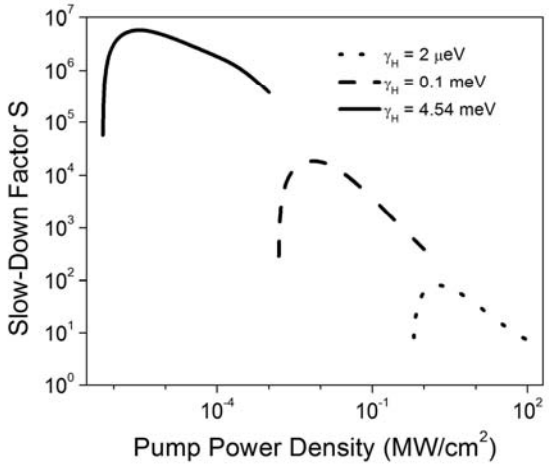

Fig. 8 Dependence of slow-down factor and the pump power density for different homogeneous linewidths.

$$S = n + \omega\frac{\partial n}{\partial\omega} = \mathrm{Re}\sqrt{\varepsilon} + \omega\frac{\partial\,\mathrm{Re}\sqrt{\varepsilon}}{\partial\omega} \tag{7}$$

If both the signal and pump detuning vanish, the slow-down factor has an analytical form as follows

$$S = \left[\frac{\varepsilon_{bac}+\sqrt{\varepsilon_{bac}^2+\varepsilon_{res}^2}}{2}\right]^{1/2}\left[1+\frac{\hbar\omega_0}{2\sqrt{\varepsilon_{bac}^2+\varepsilon_{res}^2}}\frac{U_{21}(\Omega_{PP}^2-\tilde{\gamma}_{31}^2)}{\hbar^2(\tilde{\gamma}_{31}\tilde{\gamma}_{21}+\Omega_{PP}^2)^2}\right] \tag{8}$$

where

$$\begin{aligned}U_{21} &= \Gamma|\mu_{21}|^2(f_1-f_2)/V\varepsilon_0\\ \Omega_{PP}^2 &= |\mu_{32}|^2 I_p/4\hbar^2c\varepsilon_0\sqrt{\varepsilon_{bac}}\\ \varepsilon_{res}(\Omega_{PP}^2) &= U_{21}/\hbar(\gamma_{21}+\Omega_{PP}^2/\gamma_{31})\end{aligned} \tag{9}$$

In the above, $I_p = (c/\sqrt{\varepsilon_{bac}})\varepsilon_0\varepsilon_{bac}|E_p|^2$ is the pump power density (MW/cm^2); f_1 and f_2 are Fermi-Dirac occupation factors; the difference $f_2 - f_1$ is the steady state value of the population inversion η_2.

The slow-down factor *S* as a function of pump power density is shown by Fig. 8. Three different linewidth regimes are compared. Here, we assume $\hbar\gamma_{31} = \hbar\gamma_{21}$. The homogeneous linewidth $\hbar\gamma_H$ values of 2 μeV (T = 7K), 0.1 meV (T = 75K) and 4.54 meV (T = 300K) were used for cases A, B, and C, respectively. Initially, as the pump power density increases, the slow down factor increases. This is because as the two dressed states are formed, $\mathrm{d}\,\mathrm{Re}\,\varepsilon/\mathrm{d}\omega$ changes sign from negative to positive. As the power density continues to increase, the two dressed states are farther apart and the slow down factor decreases. Hence for a given linewidth, a maximum slow down

can be attained. The slow-down factors reach maximum values of 6×10^{6} , 2×10^{4} and 82 at pump levels of 3×10^{-6} , 6×10^{-3} and 2 MW/cm^2 for cases A, B, and C, respectively. This

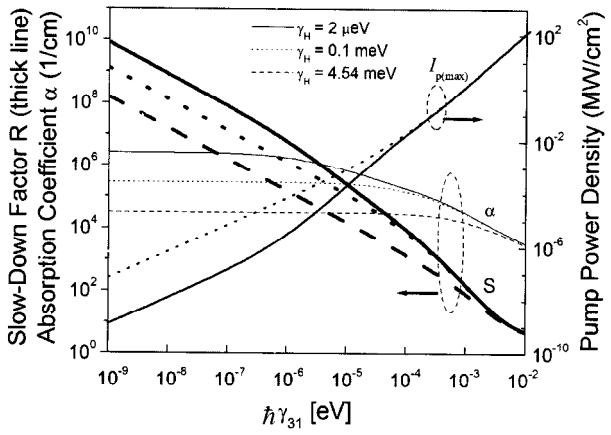

Fig. 9 Influence of $\hbar\gamma_{31}$ on slow-down factor, absorption coefficient and required pump power density at three different homogeneous linewidth regimes.

illustrates a strong dependence on the homogeneous linewidth. It is interesting to note that at higher pump density, say 100 MW/cm^2, the slow down factor for all cases approaching the same value.

Fig. 9 shows the influence of γ_{31}, if it could be independently controllable, on the slow-down factor, absorption coefficient and pump power density. All are improved with the decrease of γ_{31}. Experimentally a single QD has been shown to have μeV dephasing at low temperatures[27]. This would correspond to a slow-down factor of more than 10^7, requiring ~10 W/cm^2 pump power density. At room temperature, the dephasing linewidth $\hbar\gamma_{31}$ is 2.27meV, attributed to phonon scattering, but a slow-down factor of 82 can still be achieved. The buffer turn-on and turn-off times depend on pump power density and are of the order of a few ps (or less) for large (or small) linewidths with the above material parameters based on our transient model.

C. Slow-light in a nonuniform QD array

Experimentally, the PL measurement on a quantum dot (QD) ensemble comprised of lots of dots shows a linewidth of 20-60 meV, much larger than the homogeneous broadening linewidth. This linewidth is independent of temperature and is caused by nonuniform distribution of the dots. The nonuniformity comes from size, density, strain and composition distributions.

The slow light in a QD array involves two laser sources, the signal and the pump, nearly in resonant with two excitonic states in QDs. Due to the nonuniformity of QDs, the signal and the pump will experience different detuning when interact with different dots. Hence the overall slow down factor will be reduced. The signal wavelength is fixed by the application and the signal detuning will be unavoidable for some of the QDs.

The dielectric constant experienced by a signal as given in (6) is a function of both signal and pump detuning. This is shown in Fig. 10 where the signal and pump detuning are adjusted separately. Since Δ_s appears twice in the denominator of (6) (Δ_s

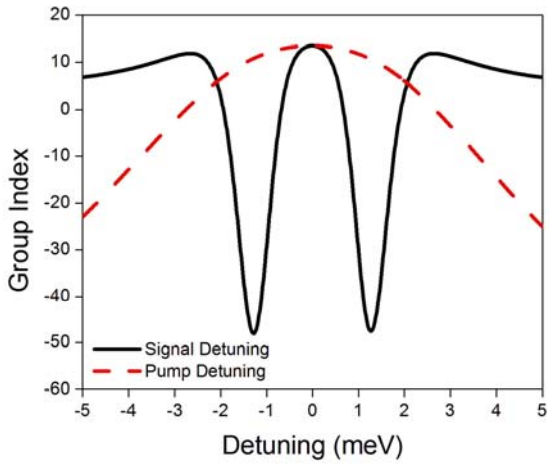

Fig. 10 The dependence of group-index seen by the signal versus both the signal (Δ_s) and the pump (Δ_p) detuning. The signal detuning has more pronounced effects on the group index. In this plot, γ_{21} and γ_{31} are 1meV. The pump power density is 2MW/cm^2.

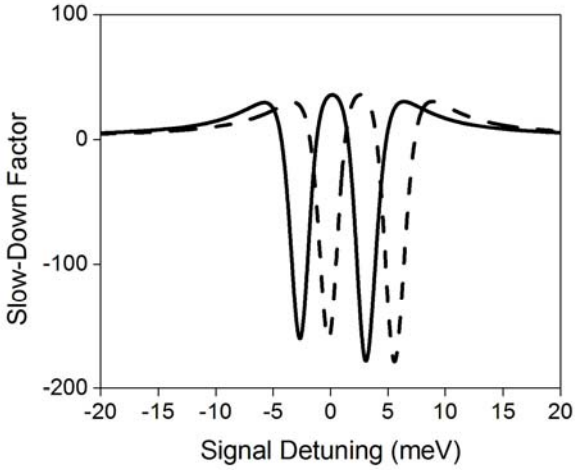

Fig. 11 Slow down factor vs. signal energy for two QD sizes with fixed signal and pump wavelengths aligned to one size. The dashed line is for the misaligned size.

appears in both $\tilde{\gamma}_{21}$ and $\tilde{\gamma}_{32}$), the dependence on Δ_s is stronger. On the other hand, slow down factor also decreases with increasing pump detuning Δ_p.

It is perhaps easy to see that if one single wavelength pump source is used, the slow down factor can be drastically reduced due to inhomogeneous broadening. In Fig. 11, we show the slow down factor schematically for a case when there are two distinct QD sizes and the pump and signal wavelengths are

aligned with one only. The slow down factor for the misaligned case is shown by the dashed curve. As can be seen here, at the signal energy, the slow down factor for the misaligned case can even be negative and hence canceling the positive slow down for the aligned QDs.

Given the above, we propose a multi-color pump scheme in which the pump is comprised of many discrete frequency components. Each component will have different powers to optimize the performance. Schematically, with this new pumping scheme, Fig. 12 shows the slow down factor for the same two-size QD case mentioned above. In this case, although the misaligned QDs would not contribute to a maximum slow down, the degradation effect can be substantially reduced.

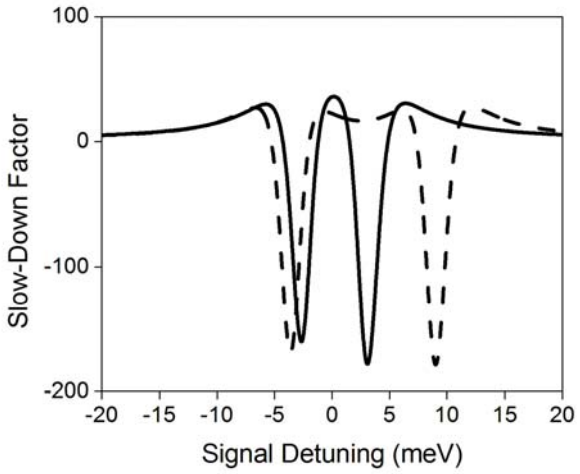

Fig. 12 Slow down factor vs. signal energy for two QD sizes with fixed signal and two pump wavelengths having different pump powers. The dashed line is for the misaligned size.

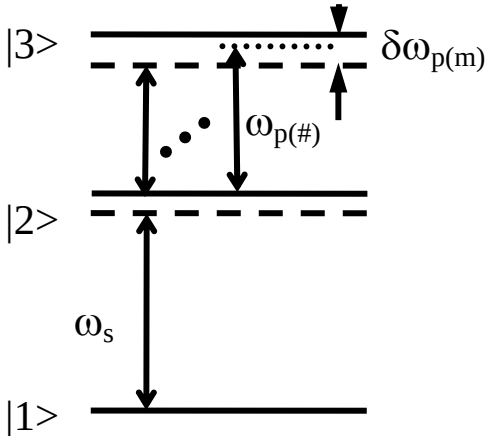

Fig. 13 Schematic of a multi-color pump scheme with a pump source comprising of several discrete components. The most resonant pump component is marked by (#).

To model the multi-color pump scheme, we use the same energy diagram as used in the case of uniform QD arrays. Particular attention is paid towards tracking the detuning values, as well as, developing formula to track multiple pumps with different detuning. With the pump source composed of $2N+1$ multi-frequency components $\omega_P^{(m)}$ ($m=-N\cdots N$) as shown in Fig. 13, the equations of motion are similar to (3) and (4). For

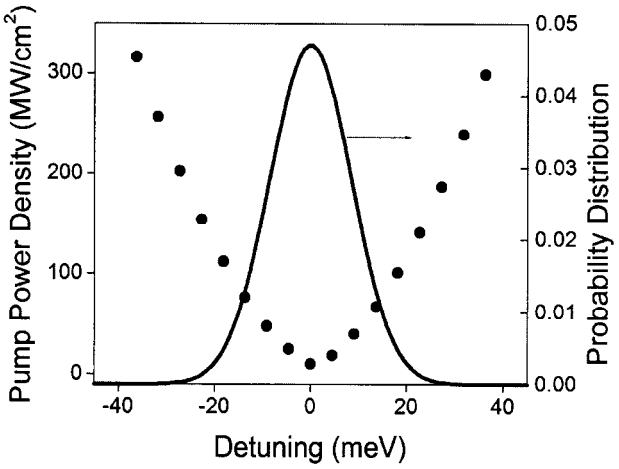

Fig. 14 Pump power density for each pump components at differnet detuning. The spacing between two adjacent pump components is 2.27meV in this plot. The solid curve shows the probablity of finding a particular group of QD with energy levels deviated from the average value of the whole ensemble by the amount determined from the x-axis.

example, the equation for σ_{21} for a particular group of QD is now

$$\dot{\sigma}_{21} = -\tilde{\gamma}_{21}\sigma_{21} - i\Omega_S\eta_2 + i\sigma_{31}\sum_m \Omega_{Pm}^* e^{-i(\omega_P^{(\#)}-\omega_P^{(m)})t} \qquad (10)$$

where $\Omega_{Pm} = \mu_{32}E_m/2\hbar$. The superscript index (#) denotes the most resonant pump component to this particular group of QDs.

If we only keep the most-resonant term in the summation, say $m=n$ and neglect all the slowly-varying exponential time factor, we obtain

$$\dot{\sigma}_{21} = -\tilde{\gamma}_{21}\sigma_{21} - i\Omega_S\eta_2 + i\sigma_{31}\Omega_{Pn}^* \qquad (11)$$

This approximation is valid if we consider steady-state solutions in which case only the longest time constant term will remain. To explicitly see this, we take Fourier transforms of (11) as follows.

$$\begin{aligned} -i\omega R_{21}(\omega) = &-\tilde{\gamma}_{21}R_{21}(\omega) + i\Omega_S(R_{11}(\omega) - R_{22}(\omega)) \\ &+ i\sum_m \Omega_{Pm}^* R_{31}(\omega - \omega_P^{(m)}) \end{aligned} \qquad (12)$$

where R_{21} is the Fourier transform of the corresponding slowly-varying density matrix σ_{21} . At steady state, only zero-frequency component contributes, that is only $R_{21}(0)$ will contribute provided the other components are far away compared to the dephasing linewidth γ_{21} . If the spacing between two adjacent pump components is less than γ_{21} (nonlinear regime), a full set of coupled nonlinear differential equations have to be solved and is under investigation. On the other hand,

if the spacing between two adjacent pump components is larger than γ_{21} (linear regime), (12) becomes

$$0 = -\tilde{\gamma}_{21} R_{21}(0) + i\Omega_S (R_{11}(0) - R_{22}(0)) + i\Omega^*_{Pn} R_{31}(0) \quad (13)$$

This justifies that the non-resonant terms at steady state don't contribute.

The solution at steady state is very similar to it is in

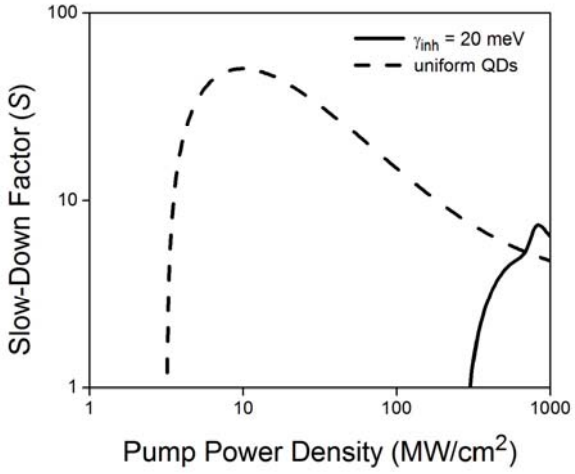

Fig. 15 Slow-down factor as a function of pump density for a single pump scheme. The QD medium has a homogeneous linewidth of 4.54 meV and inhomogeneous linewidth of 20 meV due to QD nonuniformity. The case of uniform QDs is also shown for comparison (dashed line).

subsection IV-B except now we have to carry out the explicit index label of a particular QD group. We assume EIT is reached and all the photo-created carriers will be trapped in the ground state, that is $\eta_2 \approx -1$. The (dimensionless) macroscopic dielectric constant experienced by the signal field is given by

$$\varepsilon \approx \varepsilon_{bac} + \int \mathrm{d}\delta\omega_{21} \frac{iU_{21}/\hbar}{(\gamma_{21} + i\delta\omega_{21}) + \Omega_{PP}^{(n)2} / (\gamma_{31} + i(\delta\omega_{21} + \Delta_P^{(n)}))} \quad (14)$$

where we have assumed the dipole moments are identical for all QD groups and

$$\Delta_P^{(n)} = \omega_{32}^{(0)} + \delta\omega_{32} - \omega_P^{(n)}$$

$$U_{21} \simeq \Pr(\omega_{21}^{(0)}) \frac{\Gamma}{V} |\mu_{21}|^2 (f_1 - f_2)/\varepsilon_0 \quad (15)$$

$$\Omega_{PP}^{(n)2} = \frac{|\mu_{32}|^2 I_P^{(n)}}{4\hbar^2 c\varepsilon_0 \sqrt{\varepsilon_{bac}}}$$

As a numerical example, consider a multiple-color pump source with location for each pump component shown as the circles in Fig. 14. Each component is allowed to have different power density. Consider a 20meV inhomogeneous linewidth (also plotted as the solid line in Fig. 14 for comparison) and a homogeneous broadening linewidth of 4.54 meV (room temperature value). The rest of the parameters are the same values used in Table 1.

Fig. 15 shows the slow-down factor versus pump power density for a nonuniform QD with a single pump as compared against a uniform QD array. The single pump is aligned with the average energy separation between |2> and |3>. Significant degradation of slow down factor was obtained. The maximum slow-down factor is 82 for a uniform QD array with a homogeneous linewidth of 4.54 meV. Whereas for the case with 20 meV nonuniformity and a single pump source, the maximum slow factor factors were reduced to < 10, respectively.

On the other hand, if a multi-color pump source is used, the

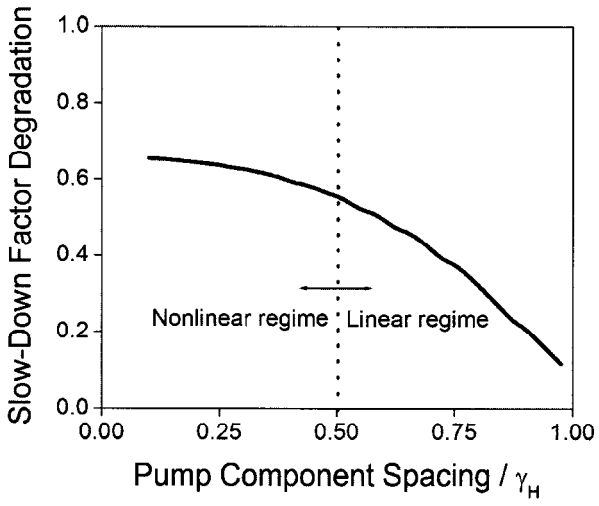

Fig. 16 Slow-down factor degradation due to QD nonuniformity.

degradation can be greatly improved. Fig. 16 shows the slow down factor degradation for a variety of pump component spacing, normalized to the homogeneous broadening linewidth $\hbar\gamma_H$. The slow-down factor degradation is defined as the ratio between the slow down factors in QD arrays with and without nonuniformity. In the calculation, we looked for a scheme to achieve the highest slow-down factor. A denser pump arrays has less degradation. The dash line represents the case the pump spacing and the homogeneous linewidth are equal. The maximum slow-down factor could still be ~40 for a nonuniform QD array with inhomogeneous linewidth of 20 meV. The optimized pump power density for each pump component is shown as the circles in Fig. 14.

D. Signal propagation through QD-based optical buffers

In this subsection, we show the effect of signal propagation through a QD based optical buffer discussed in Section III. Here, for simplicity sake, we consider only uniform QDs. We believe the nonuniformity factor can be treated simply with a slow down reduction factor, similar to what described in subsection IV-C.

In frequency domain, the output of the buffer can be related to the input signal via a system transfer function $H(\omega)$ given by

$$H(\omega) = e^{ik_z L} \quad (16)$$

where L is the length of the buffer and k_z, the propagation constant in the z (waveguide) direction is related to the dielectric constant by

$$k_z^2(\omega) = \frac{\omega^2}{c^2}\varepsilon(\omega) \tag{17}$$

For a given set of material parameters including the pump power density, we can calculate k_z and thus the transfer function $H(\omega)$. The output signal is simply the inverse Fourier transform of the product of the input signal and $H(\omega)$.

The input signal is a Gaussian pulse train with a repetition rate of 10 Gbit/s and pulse FWHM 100 ps. We set the homogeneous broadening linewidth to be 2 meV and used InAs-GaAs QDs with material parameters given in Table 1. The pump power density is fixed at 2 MW/cm^2 which corresponds to the maximum slow-down factor ~ 244. The output signal has a larger FWHM due to the non-flat frequency response. The result is shown in Fig. 17(a). The FWHM increases as the device length increases and becomes 104 ps when L is 1 cm. Fig. 17(b) shows the dependence of the total buffering capacity with the pump power density. The buffer capacity can be externally controlled via the change of the pump power. The control is continuous and can vary from 1 bit up to 87 bits[3].

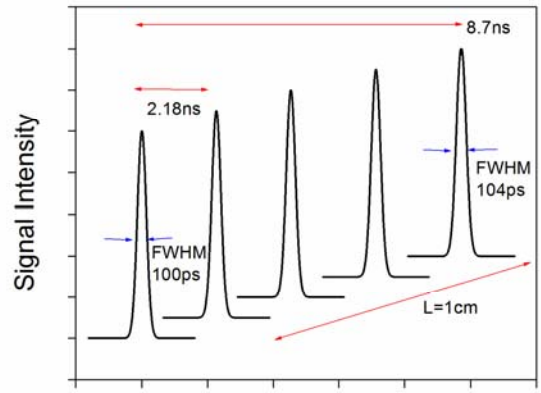

(a)

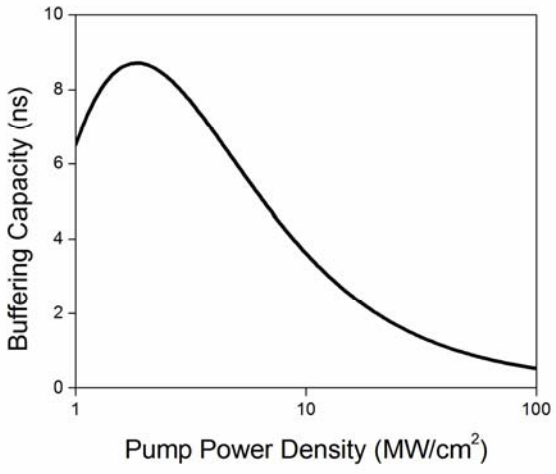

(b)

Fig. 17 (a) Signal propagation through a quantum dot waveguide with the length of 1cm. (b) Control of the slow-down factor with the pump power density.

V. Conclusion

We discussed the general principle of designing an optical buffer via slow-light. We proposed and analyzed the first semiconductor all-optical buffer based on EIT effect in QDs. The light pulses can slow down significantly with a negligible dispersion, making it desirable for making optical buffers with an adjustable storage. The effect of QD size nonuniformity is also calculated. Although the linewidth of QDs is found to be critical, our calculations show that a slow down factor of ~40 can be obtained with state-of-the-art QDs at room temperature using a novel multiple pump scheme. Our theoretical model shows that a buffering time of 8.7 ns in a 10 Gbs system could be obtained at room temperature without pulse distortion and spreading for a uniform QD waveguide. This level of storage is already interesting for a number of applications. With the improvements of QD linewidth and uniformity in the future, the slow down and storage can no doubt increase to a larger number, making them far more useful. We also anticipate that further optimization in device design and energy configuration can lead to significantly increased slow down factor. We believe an optical buffer would serve as a critical catalyst to trigger new architectures and applications in optical networks, communications, and signal processing.

REFERENCE:

1. P. C. Ku, C. J. Chang-Hasnain, J. Kim, and S. L. Chuang, *OSA Annual Meeting*, Tucson, AZ (2003).
2. P. C. Ku, C. J. Chang-Hasnain, and S. L. Chuang, *Electron. Lett.*, vol. 38, no. 24, pp. 1581-1583, November 2002.
3. P. C. Ku, C. J. Chang-Hasnain, J. Kim, and S. L. Chuang, *Optical Fiber Conference 2003*, March 2003, Atlanta GA.
4. S. E. Harris, *Phys. Today*, vol. 50, no. 7, pp. 36-42, July 1997.
5. J. P. Marangos, *J. Modern Opt.*, vol. 45, no. 3, pp. 471-503, March 1998.
6. M. Sargent III, *Phys. Rep.*, vol. 43, pp. 223-265, 1978.
7. L. V. Hau, S. E. Harris, Z. Dutton, and C. H. Behroozi, *Nature*, vol. 397, no. 6720, pp. 594-598, February 1999.
8. D. F. Phillips *et al.*, *Phys. Rev. Lett.*, vol. 86, no. 5, pp. 783-786, January 2001.
9. A. V. Turukhin *et al.*, *Phys. Rev. Lett.*, vol. 88, p.023602, January 2002.
10. M. S. Bigelow, N. N. Lepeshkin and R. W. Boyd, *Phys. Rev. Lett.*, vol. 90, p.113903, March 2003.
11. P. C. Ku *et al.*, submitted to *Phys. Rev. Lett* (2003).
12. see Special Issue on Optical Networks, *J. Lightwave Technol*., vol. 18, no. 12, December 2000.
13. P. C. Ku, *Semiconductor Slow-Light Device*, PhD Dissertation, University of California at Berkeley, 2003.
14. G. Lenz, B. J. Eggleton, C. K. Madsen, and R. E. Slusher, *IEEE J. Quantum Electron.*, vol. 37, p.525, April 2001.
15. J. B. Khurgin, *Phys. Rev. A*, vol. 62, 013821, July 2000.
16. R. Langenhorst *et al.*, *J. Lightwave Technol*., vol. 14, no. 3, pp. 324-335, March 1996.
17. J. Faist, F. Capasso, C. Sirtori, K.W. West, and L.N. Pfeiffer, *Nature*, vol. 390, p.589, December 1997.
18. C. C. Phillips *et al.*, *Physica E*, vol. 7, no. 1-2, p.166, April 2000.
19. H. Schmidt, K.L. Campman, A.C. Gossard, and A. Imamoglu, *Appl. Phys. Lett.*, vol. 70, p.3455, June 1997.
20. M. Phillips and H. Wang, *Phys. Rev. Lett.*, vol. 89, p.186401, October 2002.
21. D. Bimberg *et al.*, *Thin Solid Films*, vol. 267, no. 1-2, pp. 32-36, October 1995.

22. J. M. Moison *et al.*, *Appl. Phys. Lett.*, vol. 64, no. 2, pp. 196-198, January 1994.
23. F. Heinrichsdorff *et al.*, *Appl. Phys. Lett.*, vol. 68, no. 23, pp. 3284-3286, June 1996.
24. N. N. Ledentsov *et al.*, *Appl. Phys. Lett.*, vol. 69, no. 8, pp. 1095-1097, August 1996.
25. F. Heinrichsdorff *et al.*, *Appl. Phys. Lett.*, vol. 71, no.1, pp. 22-24, July 1997.
26. K. Mukai, N. Ohtsuka, H. Shoji, and M. Sugawara, *Appl. Surf. Sci.*, vol. 112, pp. 102-109, March 1997.
27. C. J. Chang-Hasnain, P. C. Ku, J. Kim, and S. L. Chuang, *Proc. IEEE*, vol. 9, p.1884, November 2003.
28. P. Borri *et al.*, *Phys. Rev. Lett.*, vol. 87, 157401, October 2001.
29. P. Borri *et al.*, *Phys. Rev. B*, vol. 60, pp. 7784-7787, June 1999.